Supporting Information

Reversible Bonding in Thermoplastic Elastomer Microfluidic Platforms for Harvestable 3D Microvessel Networks

Byeong-Ui Moon*[1,2], Kebin Li[1,2], Lidija Malic[1,2,3], Keith Morton[1,2], Han Shao[4], Lauren Banh[5,6,7], Sowmya Viswanathan[5,6,7], Edmond W.K. Young[4,5] and Teodor Veres*[1,2,4]

[1]*Medical Devices, Life Sciences Division, National Research Council of Canada, Boucherville, QC J4B 6Y4, Canada*

[2]*Center for Research and Applications in Fluidic Technologies (CRAFT), Toronto, ON M5S 3G8, Canada*

[3]*Department of Biomedical Engineering, McGill University, Montreal, QC H3A 2B4, Canada*

[4]*Department of Mechanical & Industrial Engineering, University of Toronto, Toronto, ON M5S 3G8, Canada*

[5]*Institute of Biomedical Engineering, University of Toronto, Toronto, ON M5S 3G9, Canada*

[6]*Osteoarthritis Research Program, Division of Orthopedic Surgery, Schroeder Arthritis Institute, University Health Network, ON M5T 0S8, Canada*

[7]*Krembil Research Institute, University Health Network, ON M5T 0S8, Canada*

**Co-corresponding authors:*
E-mails: Ben.Moon@nrc-cnrc.gc.ca, Teodor.Veres@cnrc-nrc.gc.ca

Table S1. Comparison study of oxygen permeability in various materials from literature search

References	PDMS	TPE	PS
Robb.[1] 1968	-	-	0.12 Barrer
Merkel et al.[2] 2000	800 Barrer (33% silica filler)	-	-
Lamberti et al.[3] 2014	42-131 Barrer (5:1 mixing ratio) 270-573 Barrer (10:1 mixing ratio) 950-1502 Barrer (20:1 mixing ratio)	-	-
Domansky et al.[4] 2017	-	8.9 Barrer (Kraton G1645)	-
McMillan et al.[5] 2021	563 Barrer	4.04 Barrer (Fluoroflex)	-

1 Barrer = 10^{-10} cm^3 (STP) · cm/cm^2 · s · cm Hg.

Table S2. Literature search of the TPE-based microfluidic devices for cell culture and organ-on-a-chip applications

References	Device characteristics	Fabrication method	Cell culture
Didar et al.[6]	Multilayer microfluidic device for fluidic control	Hot embossing	Oligodendrocyte progenitor cells on chip separation
Borysiak et al.[7] 2013	Modified TPE materials with polystyrene content	Liquid TPE replica molding	3T3 fibroblasts and bovine pulmonary arterial endothelial cells on the substrate
Domansky et al.[4] 2017	TPE-TPE thermal bonding	Injection molding and extrusion	Lung epithelial NCI-H441 cells, HUVECs and others cells on the substrate
Lachaux et al.[8] 2017	TPE-TPE thermal bonding	Hot embossing	DC 450 yeast cells cell growth and division
Lachaux et al.[9] 2019	TPE membrane-TPE thermal bonding	Spin coating process on the epoxy molding	Mononuclear cell culture for adhesion and proliferation
Schneider et al.[10] 2021	Polycarbonate/TPE-glass microfluidic device	Hot embossing	HUVECs monolayer
Schneider et al.[11] 2021	TPE-PMMA thermal fusion bonding	Hot embossing	HUVECs culture and monitoring cell metabolism
Our work	TPE-PS thermal bonding	Hot embossing	FBs and HUVECs for 3D vessel networks

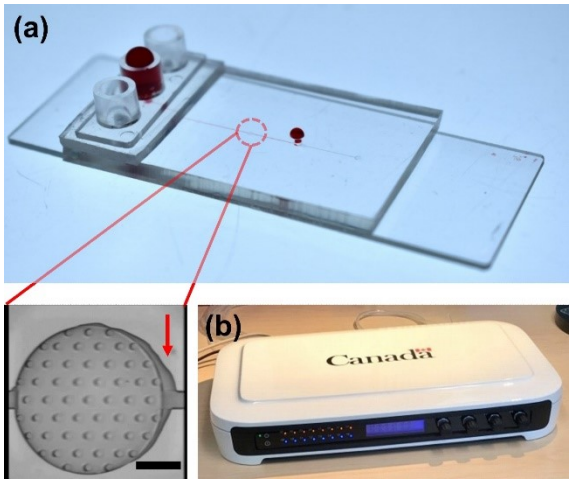

Figure S1. Bonding strength measurements. (a) A photograph of an assembled device for delaminating pressure testing. As the applied pressure increases, the TPE chamber begins to delaminate from the PS substrate, as indicated by a red arrow (inset). The scale bar is 200 μm. (b) An in-house-built pneumatic pressure testing box equipped with pressure regulation channels.

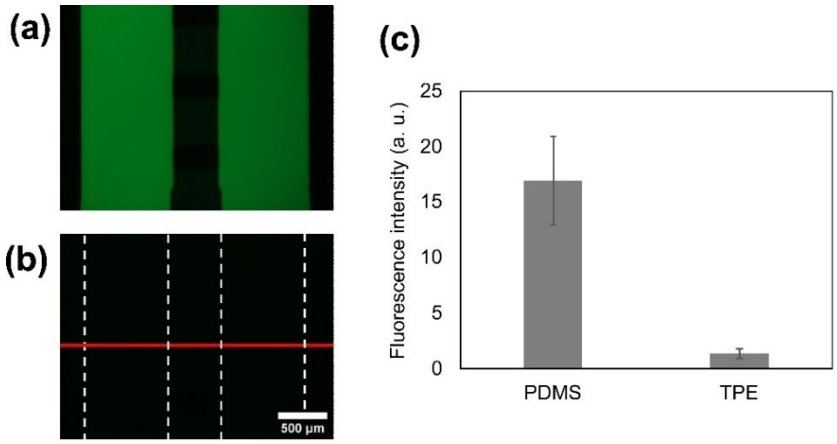

Figure S2. Protein absorption study on the PDMS and TPE channels. Two identical microfluidic channels were prepared on both PDMS and TPE slabs and bonded to the glass slide substrate. (a) We introduced a concentration of 1 mg/mL FITC-Dextran (molecular weight 75 kDa) into the devices and incubated them at 37 ºC for 5 hr. After the washing step, we captured fluoresce images (b) with PDMS channels and TPE channels. The dashed white lines represent microchannels and the red lines represent a plot line of the fluorescent intensity. (c) Comparison graph of the protein absorption. The PDMS channels show significantly higher protein absorption on the surface compared to the TPE channels (n=6 different channels).

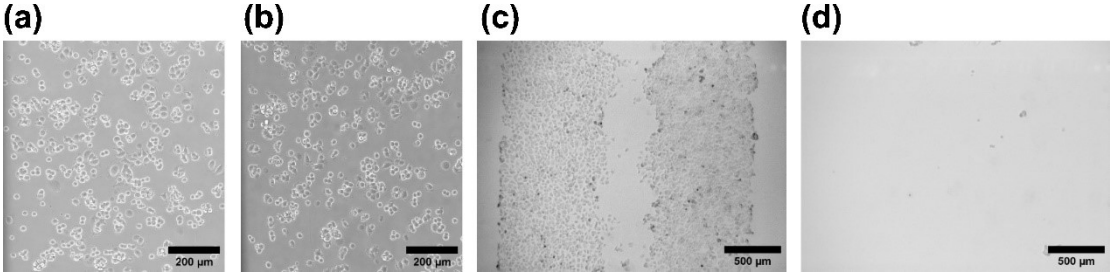

Figure S3. TPE-based microfluidic cell culture. Images of MCF-7 cell seeding on different TPE-PS devices (a and b) show the same cell seeding density, with approximately 8,000 cells seeded on each side of the wells. Bright-field images of the patterned cells on the PS substrate after TPE slab removal (c) and after trypsinization (d). A note that the image (d) has a different scale bar compared to Fig. 2(h) in the main text.

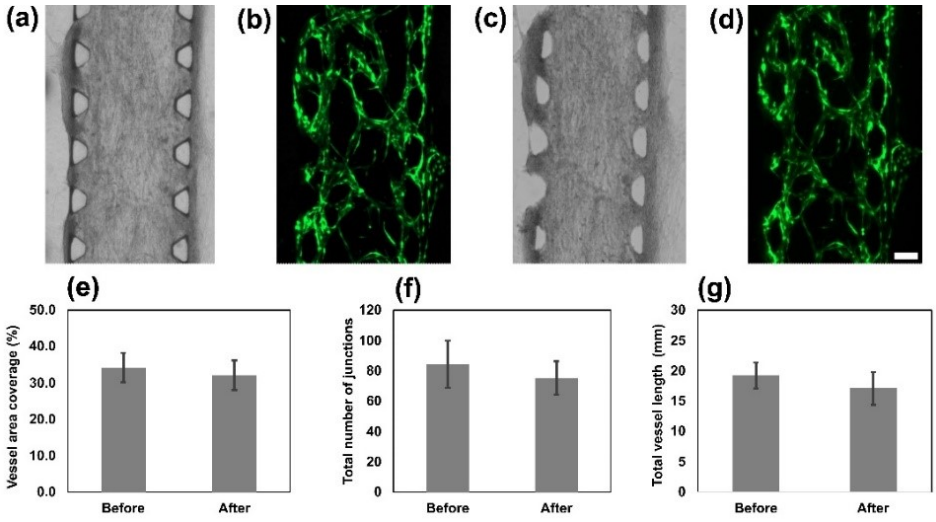

Figure S4. Microfluidic-engineered microvessel network structures before (a and b) after (c and d) TPE slab removal. Cultured tissue images of bright-field (a and c) and fluorescence (b and d). Upon TPE slab removal (c and d), the tissue remains intact and the vessel network stays on the PS dish and without damaging vessel networks. (e-g) Comparative analysis of vessel area coverage, total number of vessel network junctions and total vessel length before and after TPE removal. There is no significant difference before and after the TPE removal. (N = 3; mean ± SD). The scale bar is 200 µm.

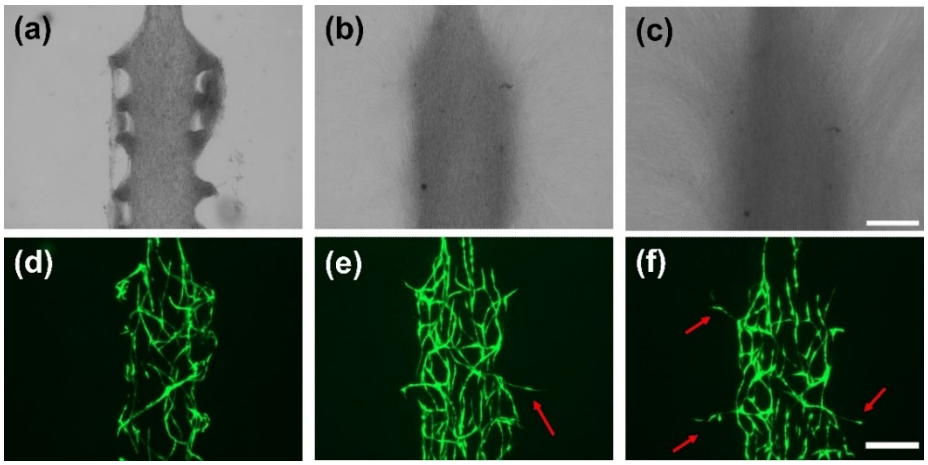

Figure S5. Bright-field images of tissue growth after TPE slab removal (a) after removal, (b) 2 days and (c) 4 days of culture and fluorescence images of the microvessel networks (d-f), respectively. Following the TPE removal, the tissue continued to grow outward from the pattern area. Red arrows indicate microvssel growth outside of the patterned area. A note that here, there is no flow and the culture media is an under static flow condition. The scale bars are 500 μm.

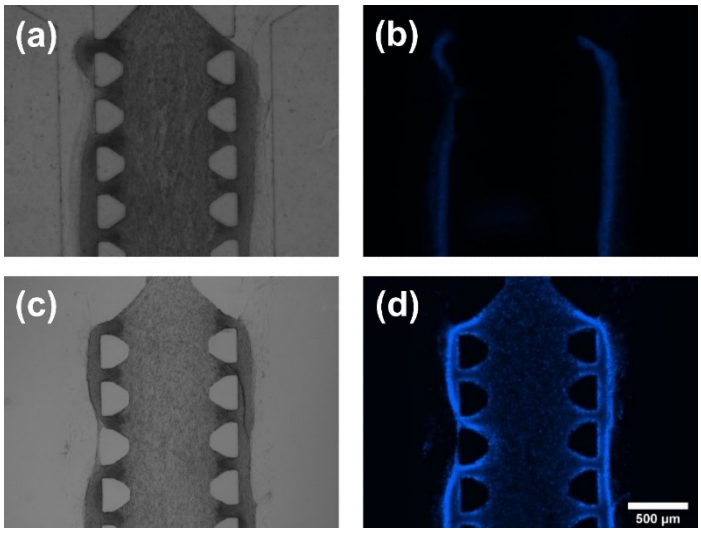

Figure S6. A proof-of-principle experiment to demonstrate the difference between staining with irreversibly bonded PDMS devices (a-b) vs. accessible 3D tissue staining after TPE slab removal (c-d). Note there are no open ports and the microvessel networks are not in a perfusable condition in both conditions. (a) An irreversibly-bonded PDMS-glass microfluidic device. (b) Fluorescence image showing only the tissue near channel boundaries are stained due to lack of access of staining solution to tissue core. (c) A reversibly-bonded TPS-PS microfluidic device after the TPE slab removal. (d) Fluorescence image showing that the entire tissue on the PS substrate was fully stained.

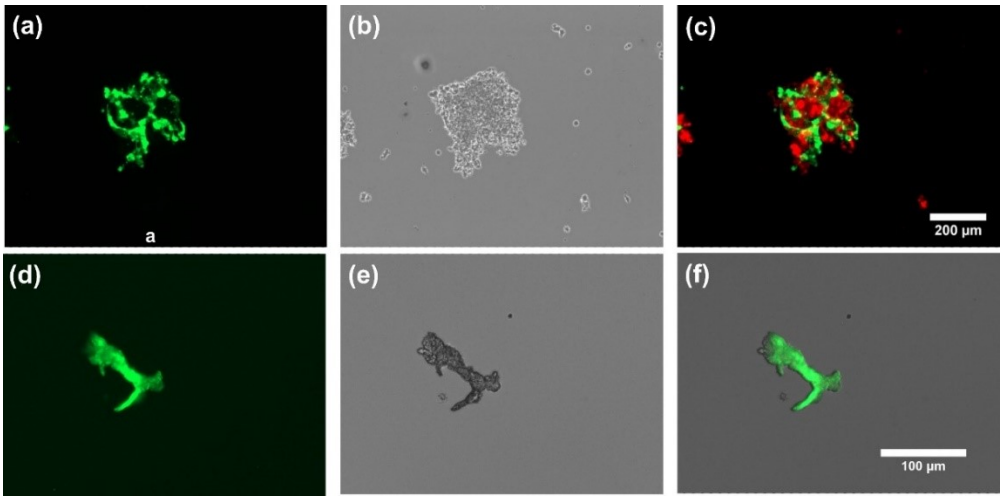

Figure S7. Images of harvested microvessel segments with fibroblasts (a-c) and microvessel fragments (b-d). Microvessel segments are shown in GFP images (a, d), bright-field images (b, e), and merged images (c, f). The tissue digestion process involves tissue collection from the microfluidic devices, and dissociating it in a BAS-PBS solution containing Collagenase type I (2 mg/mL) and DNase I (1 mg/mL). Throughout the centrifugation step, the dissociated segments were pooled and collected for imaging.

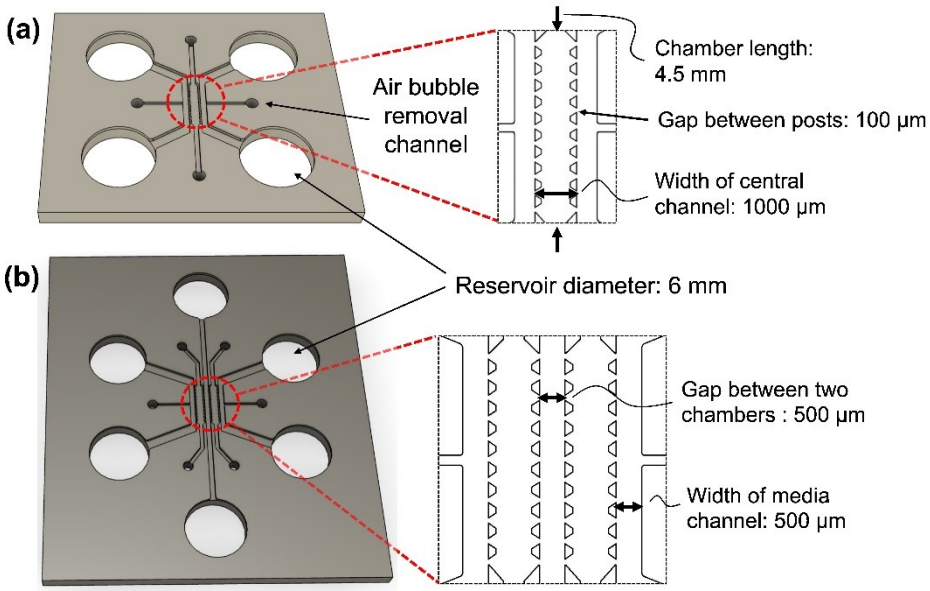

Figure S8. Designs of (a) single vessel loading and (b) multi-vessel loading chambers. Key dimensions of TPE slabs are depicted as: width of the cell loading channel = 1000 µm, width of the media flowing channels = 500 µm, gap between posts = 100 µm, gap between two chambers of the multi-vessel loading design = 500 µm, length of the chamber = 4.5 mm, reservoir diameter = 6 mm, inlet and outlet diameters = 1 mm, and height of the channel = 130 µm.

References:

1 W. L. Robb, *Ann. N. Y. Acad. Sci.*, 1968, **146**, 119–137.

2 T. C. Merkel, V. I. Bondar, K. Nagai, B. D. Freeman and I. Pinnau, *J. Polym. Sci., Part B: Polym. Phys.*, 2000, **38**, 415–434.

3 A. Lamberti, S. L. Marasso and M. Cocuzza, *RSC Adv.*, 2014, **4**, 61415–61419.

4 K. Domansky, J. D. Sliz, N. Wen, C. Hinojosa, G. Thompson, J. P. Fraser, T. Hamkins-Indik, G. A. Hamilton, D. Levner and D. E. Ingber, *Microfluid. and Nanofluidics*, 2017, **21**, 107.

5 A. H. McMillan, J. Mora-Macías, J. Teyssandier, R. Thür, E. Roy, I. Ochoa, S. De Feyter, I. F. J. Vankelecom, M. B. J. Roeffaers and S. C. Lesher-Pérez, *Nano Select*, 2021, **2**, 1385–1402.

6 T. F. Didar, K. Li, T. Veres and M. Tabrizian, *Biomaterials*, 2013, **34**, 5588–5593.

7 M. D. Borysiak, K. S. Bielawski, N. J. Sniadecki, C. F. Jenkel, B. D. Vogt and J. D. Posner, *Lab Chip*, 2013, **13**, 2773–2784.

8 J. Lachaux, C. Alcaine, B. Gómez-Escoda, C. M. Perrault, D. O. Duplan, P. Y. J. Wu, I. Ochoa, L. Fernandez, O. Mercier, D. Coudreuse and E. Roy, *Lab Chip*, 2017, **17**, 2581–2594.

9 J. Lachaux, H. Salmon, F. Loisel, N. Arouche, I. Ochoa, L. L. Fernandez, G. Uzan, O. Mercier, T. Veres and E. Roy, *Adv. Mater. Technol.*, 2019, **4**, 1800308.

10 S. Schneider, E. J. S. Brás, O. Schneider, K. Schlünder and P. Loskill, *Micromachines*, 2021, **12**, 575.

11 S. Schneider, M. Bubeck, J. Rogal, H. J. Weener, C. Rojas, M. Weiss, M. Heymann, A. D. van der Meer and P. Loskill, *Lab Chip*, 2021, **21**, 3963–3978.